Coumarin-poly(2-oxazoline)s as synergetic and protein-undetected nanovectors for photodynamic therapy

Diana Heaugwane, Orélia Cerlati, Kedafi Belkhir, Tarek Benkhaled, Sylvain Catrouillet, Isabelle Fabing, Catherine Claparols, Marc Vedrenne, Dominique Goudounèche, Bruno Payré, et al.

International Journal of Pharmaceutics 658 (2024) 124186

Contents lists available at ScienceDirect

International Journal of Pharmaceutics

journal homepage: www.elsevier.com/locate/ijpharm

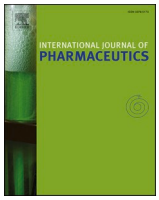

Coumarin-poly(2-oxazoline)s as synergetic and protein-undetected nanovectors for photodynamic therapy

Diana Heaugwane [a], Orélia Cerlati [a], Kedafi Belkhir [b], Belkacem Tarek Benkhaled [b], Sylvain Catrouillet [b], Isabelle Fabing [c], Catherine Claparols [d], Marc Vedrenne [d], Dominique Goudounèche [e], Bruno Payré [e], Beatrice Lucia Bona [f], Alice Tosi [f], Francesca Baldelli Bombelli [f], Patricia Vicendo [a], Vincent Lapinte [b], Barbara Lonetti [a], Anne-Françoise Mingotaud [a,*], Laure Gibot [a,*]

[a] *Laboratoire Softmat, Université de Toulouse, CNRS UMR 5623, Université Toulouse III – Paul Sabatier, 31062 Toulouse, France*
[b] *ICGM, Université de Montpellier, CNRS, ENSCM, Montpellier, France*
[c] *Laboratoire SPCMIB, CNRS UMR5068, Université Toulouse III - Paul Sabatier, 118 Rte de Narbonne, 31062 Toulouse cedex 9, France*
[d] *Institut de Chimie de Toulouse, Université Toulouse 3 Paul Sabatier, ICT-FR CNRS 2599, 31062 Toulouse France*
[e] *CMEAB Université Toulouse III – Paul Sabatier, 133 Route de Narbonne, 31062 Toulouse cedex, France*
[f] *Laboratory of Supramolecular and Bio-Nanomaterials (SupraBioNanoLab), Department of Chemistry, Materials, and Chemical Engineering "Giulio Natta", Politecnico di Milano, Via Luigi Mancinelli 7, 20131 Milan, Italy*

ARTICLE INFO

Keywords:
Polymer
Self-assemblies
Poly(2-oxazoline)
Photodynamic therapy (PDT)
Coumarin
Protein corona

ABSTRACT

Because of the difficult challenges of nanopharmaceutics, the development of a variety of nanovectors is still highly desired. Photodynamic therapy, which uses a photosensitizer to locally produce reactive oxygen species to kill the undesired cells, is a typical example for which encapsulation has been shown to be beneficial. The present work describes the use of coumarin-functionalized polymeric nanovectors based on the self-assembly of amphiphilic poly(2-oxazoline)s. Encapsulation of pheophorbide a, a known PDT photosensitizer, is shown to lead to an increased efficiency compared to the un-encapsulated version. Interestingly, the presence of coumarin both enhances the desired photocytotoxicity and enables the crosslinking of the vectors. Various nanovectors are examined, differing by their size, shape and hydrophilicity. Their behaviour in PDT protocols on HCT-116 cells monolayers is described, the influence of their crosslinking commented. Furthermore, the formation of a protein corona is assessed.

1. Introduction

Over the last 30 years, polymeric nanoparticles or self-assemblies have been extensively assessed as drug nanovectors, particularly for intravenous administration, linked to the discovery in the early 80s of the so-called enhanced permeability and retention effect (EPR). The intercellular disjunction of the endothelial cells in a tumor area together with the atrophy of lymphatic system enables to bring a macromolecular or encapsulated drug efficiently with passive targeting (Das et al., 2019). Because polymer systems are often much more stable in biological media than lipidic formulations, they have been the focus of many studies. Parameters such as chemical composition, nanovector size, morphology or shape have been extensively examined and all were shown to induce possible different effects (Coty and Vauthier, 2018; Qin and Li, 2020). Added to the intrinsic variability of the biological environment, nanomedicine is still nowadays far from understanding all aspects of the domain (Kaur et al., 2022). In order to benefit from EPR, nanovectors must remain in the blood circulation for approximately 2 days. Linked to this need, people have increasingly examined the interaction of the nanovectors with the components of the biological fluids. It has been known for a long time that any foreigner particle or body can be recognized by specific proteins such as opsonins. This recognition step induces efficient clearance of the foreigner through the mononuclear phagocyte system. However, beyond this opsonization process, nanovectors have been shown to possibly interact with various types of proteins, without necessarily inducing their rapid clearance

* Corresponding authors.
E-mail addresses: anne-francoise.mingotaud@cnrs.fr (A.-F. Mingotaud), laure.gibot@cnrs.fr (L. Gibot).

https://doi.org/10.1016/j.ijpharm.2024.124186
Received 22 February 2024; Received in revised form 29 April 2024; Accepted 29 April 2024
Available online 1 May 2024

(Rampado et al., 2020). This has been the starting point of a huge interest in the protein corona of the vectors (Zeng et al., 2019; Cagliani et al., 2019; Escamilla-Rivera et al., 2019; Wang et al., 2023). Understanding this corona is essential for nanomedicine because exposure of the nanovectors to biological medium inevitably leads to their contact with proteins. Therefore, their fate is linked to this possible interaction and protein corona evaluation is a fundamental step during their design for the development of stealth systems in order to obtain the protein fouling property (Monopoli et al., 2011; Ren et al., 2022). Going beyond these, protein adsorption might be a desirable process in some cases, where the protein corona might be used as a targeting tool (Ritz et al., 2015; Schöttler et al., 2016; Danner et al., 2019; Digiacomo et al., 2020; Gatti et al., 2023).

Linked to the need of long circulation, researchers have also been looking for ways to extend the nanovectors stability in the bloodstream. One suggested method, already tested for lipidic formulations, uses crosslinking. Indeed, this prevents dissociation of the vector which can then possibly travel long enough to find its targeted site. Several examples have shown that such a strategy is indeed efficient (Fan et al., 2019; Rijcken et al., 2022). Different chemistries may be used to crosslink the vectors, such as radical polymerization, glutaraldehyde reaction with amine groups or photoinitiated reactions. In this last category, dimerization of functional molecules upon illumination provides an elegant method to precisely control the time of reaction without adding any new chemicals which might be problematic for biological applications. Among all photoinitiated dimerization of small molecules, that of coumarin has been the subject of many studies. Indeed, as a small molecule, coumarin and its derivatives are known to exhibit a lot of beneficial properties: anticoagulant, antibacterial, anti-inflammatory, antioxidant, antitumor or antiviral (Al-Warhi et al., 2020; Annunziata et al., 2020; Garg et al., 2020; Küpeli Akkol et al., 2020). However, at high doses, coumarin becomes hepatotoxic. Coumarin also exhibits the possibility to dimerize upon UV illumination. This is largely used in chemistry to synthesize elaborate and functional molecules. As tunable chemical groups, coumarin moieties have also been incorporated in polymers, to lead to photoresponsive systems (Chang et al., 2015; Korchia et al., 2015, 2017; Cazin et al., 2021). Remarkably, coumarin is also known to be a photosensitizer for photodynamic therapy (PDT) (Ortega-Forte et al., 2021). PDT implies the *in situ* generation of reactive oxygen species (ROS) following illumination of a photosensitizer and transfer of its energy to the surrounding oxygen molecules (Verger et al., 2021). This oxidative stress consequently leads to cell death. PDT is used clinically in dermatology, ophthalmology, or oncology. In the recent years, low molecular weight coumarins have been evaluated as photosensitizers for PDT. Ten years ago, Wu and coll. proposed several coumarin derivatives modified by oligo(ethylene glycol) chains (Zou et al., 2013). They were all efficient on HepG2 cells, and interestingly two of them were also active as 2-photon sensitizers. In a similar manner, Li and coll. described coumarin derivatives of various hydrophilicities exhibiting NIR emission (Zhao et al., 2020). They were shown to rapidly interact with cellular membranes. An improved interaction with mitochondria led to a good PDT behaviour. Marchan and coll. subsequently thoroughly characterized similar coumarin products and showed that cell death was induced by simultaneous autophagy and apoptosis (Ortega-Forte et al., 2021). In a latter study, they reported that the PDT efficiency was improved when the coumarin derivatives were encapsulated in polyurethane – polyurea nanocapsules (Bonelli et al., 2022). In our team, we have formerly thoroughly characterized PDT using Pheophorbide a (Pheo) as photosensitizer and showed that encapsulating it in polymer self-assemblies strikingly improved its efficiency, linked to a better dispersion (Gibot et al., 2014; Knop et al., 2009; Montis et al., 2018; Till et al., 2016b). Encapsulation of photosensitizers has been assessed widely in literature in order to improve biodistribution and limit the intrinsic photosensitivity existing for the patient (Grünebaum et al., 2015; Obaid et al., 2016; Schoppa et al., 2021). Beyond encapsulation, covalent grafting of photosensitizers to nanovectors has been also assessed (Tian and Zhang, 2019; Velychkivska et al., 2022). This is another path, which however implies the stability of the photosensitizer during all process steps following grafting, and which also links the fate of the porphyrin to that of the vector. In our case, working with Pheo, covalent grafting was not examined as a possibility mainly because the presence of Pheo is not compatible with the crosslinking procedure under UV irradiation. In 2019, we evaluated the potential of a coumarin-based poly(2-methyl-2-oxazoline) derivative in PDT and showed that it was able, in a crosslinked form, to efficiently encapsulate Pheo and lead to good PDT results (Oudin et al., 2019). However, this preliminary study dealt with only one polymer, the hydrophobicity of which was limited. We therefore present here a more thorough study extending to different amphiphilic poly(2-oxazoline)s and compare their behaviour in PDT treatment knowing that poly(2-oxazolines) exhibit a stealth behavior consequently to their high water solubility, cytocompatibility, hematocompatibibity, degradability and acting as immunomodulator (Lorson et al., 2018). This is the occasion to also evaluate the input brought by the coumarin unit and the presence of a possible protein corona.

2. Materials and methods

2.1. Materials

4-Methylumbelliferone (4-MU) was purchased from Sigma Aldrich and used without further purification. Pheophorbide a was purchased from Frontier Scientific, characterized by UHPLC/MS and NMR (Fig S1-S6), and used as received. All other commercial reagents and solvents were used as received. The polymers CoumPhOXA$_m$-MOXA$_n$, CoumBuOXA$_m$-MOXA$_n$ and the X2080 crosslinker were synthesized according to already published procedures (Belkhir et al., 2022) and showed in Scheme 1. MePhOXA$_{31}$-MOXA$_{65}$ was produced by using the same protocol and MeOTs as cationic ring opening polymerization initiator (Figures S1 and S2). Ultrapure water was obtained from an ELGA Purelab Flex system (resistivity greater than 18.2 MΩ.cm) and was filtered on 0.2 μm RC filters just before use. Fetal Bovine Serum (FBS) (TMS-013) and β-mercaptoethanol purchased from Merck. Dulbecco's modified eagle medium (DMEM) was purchased from Gibco Life Technologies.

2.1.1. Formation of polymer self-assemblies by film rehydration

10 Mg of polymer and the desired amount of crosslinker (calculated as 1/1 mol/mol of coumarin units between POXA and the crosslinker) were dissolved in 0.4 mL of chloroform. The solvent was then removed on a rotary evaporator for 1 h. The polymer film formed was dried further in a vacuum at room temperature overnight. 4 mL of filtered water was then added, and the suspension was heated at 65 °C for 30 min, followed by ultrasonication at 65 °C for 1 h.

2.1.2. Coumarin dimerization

A 5-mm glass tube containing 2.2 mL of the self-assembly solution was placed at 8 mm between two UV lamps for 12 h, Philips linear T5 8 W, irradiation at 360 nm, lamp-tube distance 8 mm, total irradiance 1.0 mW cm^{-2}, measured with an HD9021 photometer from Delta Ohm Inc.

2.1.3. Preparation of Pheo and 4-MU solutions

Both solutions were prepared by nanoprecipitation. Namely, Pheo and 4-MU were first dissolved in acetone at 1.7 mM and 17 mM respectively. 45 μL of the Pheo solution and 150 μL of the 4-MU one were then added over 5 min in water (5 mL for Pheo, 4 mL for 4-MU) under stirring. The solution was left under stirring for 30 min, followed by a 2-day stay under the hood without any cap on the top of the flask to let acetone evaporate. The weight of the final solution was checked and possibly adjusted with filtered ultrapure water. The solutions were then possibly diluted with filtered water to the desired Pheo and 4-MU concentration.

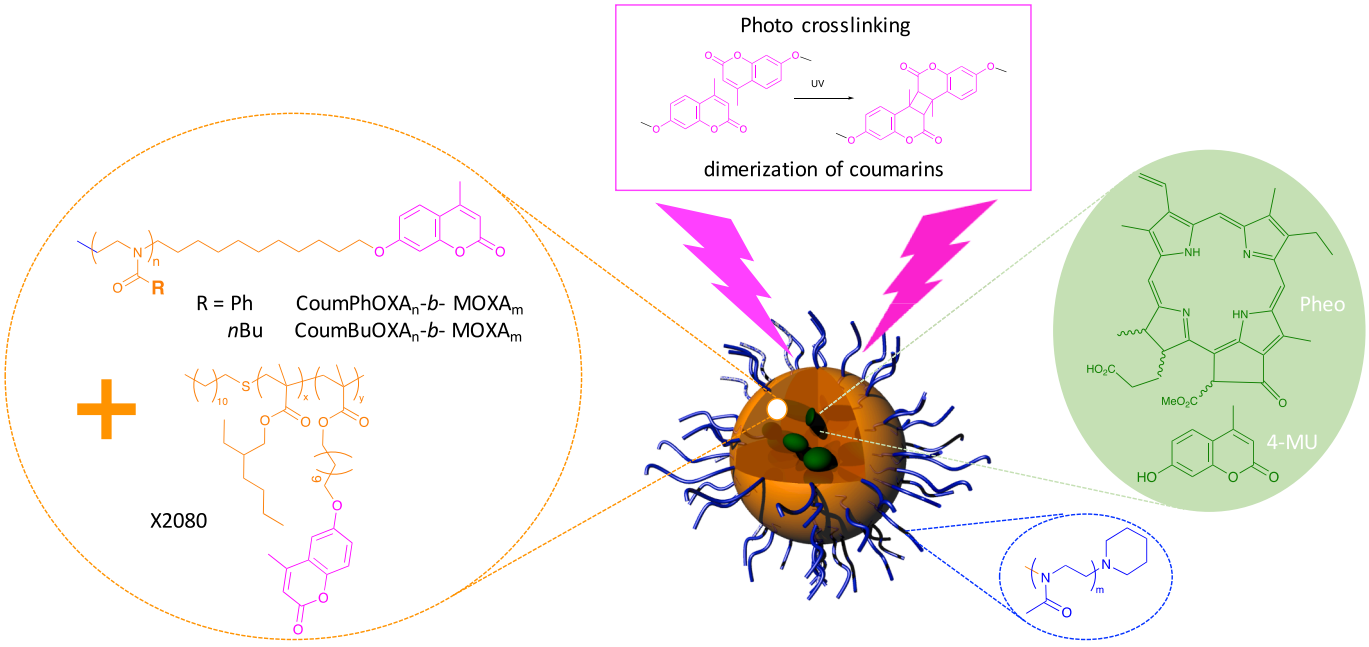

Scheme 1. Formation of the nanovectors.

2.1.4. *Encapsulation of Pheo*

A known amount of a Pheo solution in acetone was added under stirring to the polyoxazoline nanovector solution in water so that Pheo/polyoxazoline ratio was 1/30 mol/mol. The added volume was typically less than 30 μL to ensure the stability of the already present nanovectors. The solution was then left standing for 2 days to evaporate the acetone. The final weight of the solution was checked and possibly adjusted with water.

2.2. *Methods*

2.2.1. *Dynamic light scattering (DLS)*

DLS analyses were carried out at 25 °C on a Malvern (Orsay, France) Zetasizer NanoZS. The solutions were analyzed in triplicate without being filtered in order to characterize the plain samples. Data were analyzed using the general-purpose non-negative least squares (NNLS) method. The typical accuracy for these measurements was 10–20 % for systems exhibiting a polydispersity index of less than 0.4. To provide a full image of the dispersity of the results obtained between batches, intensity- and number-average results are provided for different batches of film rehydration (Figure S9). Number-average values were found to be very reproducible between batches. In some instances, intensity-average values exhibited larger values.

All correlograms were analyzed by a custom-made program named STORMS in order to obtain a more precise characterization of the solutions (Till et al., 2016a). This program was designed with Matlab, and makes it possible to fit DLS correlograms using different sets of parameters, corresponding to all hypotheses to be made during treatment. Indeed, the transition from correlograms to size results implies three levels of hypotheses: the first consists in the transformation of auto-correlation data to a diffusion coefficient, the second one involves extracting the size of the scattering object from the diffusion coefficient based on its geometry, and, finally, a model is used enabling the transformation of the intensity-relative population to a number-relative one. For each step, STORMS provides a choice of different parameters. For the nano-objects described here, the protocol used NNLS fitting, assuming a spherical shape for all objects, and the chosen scattering model corresponded to a mixture of micelles and vesicles (maximum micelle size set to a radius of 25 nm). Different sets in respect of the range of decay rates and the regularization parameter were used, α= 5 and range = 1 being the most appropriate values for the samples from this study. Unless stated otherwise, this treatment provided residuals of less than 5×10^{-3} for all analyses. The polydispersity index (PDI) is the ratio between the variance of the distribution and the square of the mean value of the decay rate, $\bar{\Gamma}$.

2.2.2. *Transmission Electron Microscopy (TEM)*

Negatively stained specimens were prepared by first depositing droplets of dilute aqueous particle suspensions onto freshly glow-discharged copper grids supporting a carbon film. After 1–3 min, the excess liquid was absorbed with filter paper and, before complete drying, a droplet of 2 wt% uranyl acetate aqueous solution was deposited. The excess stain was blotted, and the preparations were allowed to air-dry. The specimens were observed with a Hitachi HT7700 microscope operating at an accelerating voltage of 80 kV and equipped with an AMT CCD camera, or a JEOL JEM-2100 Plus microscope operating at 200 kV and equipped with a Gatan Rio16 camera. Size distribution histograms were determined by measuring the diameter of populations of about 200 particles from the TEM images, using ImageJ software. The results were expressed as mean diameters and standard deviations.

2.2.3. *Protein corona (PC)*

For protein corona studies, NPs were incubated (dilution 1:5) in DMEM + 10 % FBS for 30 min at 37 °C. Samples were characterized by DLS before and after incubation. For the isolation of NPs/PC complexes, centrifugation using a sucrose gradient was performed, adapting the protocol reported by D. Di Silvio et al (Silvio et al., 2015). Specifically, a 3–30 % sucrose gradient was prepared by layering 11 mL of the linear sucrose gradient in 13 mL tubes and left equilibrating overnight. Then 0.7 mL of samples were loaded on top of the prepared sucrose gradient solutions and subjected to ultracentrifugation (60 k rcf, 1 h), using a TH-641 rotor (Thermo Scientific) at 20 °C. After the run, aliquots of 1 mL were collected by sucking up sucrose from the top of the tubes to the bottom, dialyzed overnight at 4 °C against milliQ Water and analyzed by DLS to identify protein corona NPs. The layers containing NP/PC complexes were then concentrated by Amicon centrifugal filters (MWCO 100 kDa, Millipore) at 405 rcf to a final volume of 200 μL. 15 μL of samples were then added to 5 μL of SDS-PAGE loading buffer 2× (Laemmli buffer, Bio-Rad®, + 5 % β-mercaptoethanol), kept at 98 °C for 5 min and then loaded on a 12 % poly-acrylamide gel together with 4 μL

of a molecular ladder (Precision Plus Protein TM Standards Unstained and Dual Colors, Bio- Rad® Laboratories). Gels were developed by Silver Staining (Pierce™ Silver Stain, Thermo Fisher). DMEM + 10 % FBS without incubating NPs was used as control and subject to the same protocol used for NPs. This allowed to determine the sucrose gradient layers that were enriched in serum proteins and exclude samples contamination with free proteins in the experiment performed with NPs.

2.2.4. Cell culture

Human HCT-116 colorectal cancer cells (ATCC #CCL-247) were purchased from ATCC in 2019 and used for experiments under passage 10. Cells were grown in DMEM containing 4.5 gL^{-1} glucose, GLUTAMax, and supplemented with 10 % of heat-inactivated FBS, 100 U/mL penicillin, and 100 $\mu g \cdot mL^{-1}$ streptomycin. Cells were maintained at 37 °C in a humidified atmosphere containing 5 % CO_2. Throughout the experiments, cells were tested negative for mycoplasma (MycoAlert mycoplasma detection kit, Lonza).

2.2.5. Cytotoxicity and phototoxicity of Pheo-loaded polymeric nanovectors

Human HCT-116 tumor cells were seeded in 96-well plates (4,000 cells per well) 24 h prior to experiment. Firstly, cytotoxicity of empty or pheo-loaded (1/30 mol/mol) polymer self-assemblies was assessed after 24 h of cells incubation with nanovectors in a range of pheophorbide (Pheo) concentrations from 7.8 nM to 1 μM, corresponding to polymer concentrations of 234 nM to 30 μM. Secondly, to determine phototoxicity of the different types of nanovectors in a photodynamic therapy context, cells were incubated for 30 min at 37 °C with empty, pheo-loaded nanovectors or free pheophorbide as a control and then light activated as previously performed (Gibot et al., 2014; Oudin et al., 2019; Till et al., 2016b, 2016a; Zheng et al., 2023). A spotlight protected by a glass slide (band pass filter $\lambda > 400$ nm) was placed 4 cm above the samples. Cells were light-irradiated for a total of 4 min (2 min light on, 2 min light off and then 2 min light on in order to avoid heating). Each was exposed to a total of 8.2 $J.cm^{-2}$. After light irradiation, the cells were placed back in the incubator until analysis. Cell viability was then assessed using PrestoBlue reagent (Invitrogen) according to the manufacturer's instructions. In brief, after 24 h of incubation with nanovectors, cell culture medium was removed and cells were incubated for 30 min at 37 °C with 100 μL of 1X PrestoBlue reagent diluted in PBS before reading fluorescence at 560/590 nm on a plate reader (Synergy H1, Biotek, Winooski, VT, USA). For every set of independent experiments, six biological replicates were produced and analyzed. The full list of polymer nanovectors tested in cell biology experiments is described in Table 1.

2.2.6. Statistical analyses

Six biological replicates were produced and analysed for each independent experiment. Data analysis was performed using GraphPad Prism 8 (GraphPad Software, Inc., La Jolla, CA, USA), and independent biological replicates were plotted and expressed as mean ± SEM (standard error to the mean). Statistical comparisons were performed using one-way analysis of variance (ANOVA), followed by a Tukey's Multiple Comparison Test which compare each condition with every other condition. Overall statistical significance was set at *$p < 0.05$, **$p < 0.01$, ***$p < 0.001$, and ****$p < 0.0001$.

3. Results and discussion

3.1. Preparation of the nanovectors

The synthesis of all polymers was already described and is based on the cationic ring-opening polymerization of 2-alkyl-2-oxazolines. The formation and characterization of the self-assemblies in water has also been the subject of a thorough publication as illustrated in Scheme 1 (Belkhir et al., 2022). Basically, the formulation included the addition of

Table 1
List and description of the empty or pheo-loaded self-assemblies used in the study (Belkhir et al., 2022). For the naming of each system, /X2080 indicates that the crosslinker was present, the presence of X in front of the name indicates that the system was crosslinked. (Pheo) in front of the name indicates that Pheo was added to the nanovector. * low number of objects typically means that less than 50 objects could be observed.

Notation	Description	Characteristics*
Pheo	Free pheophorbide	200 nm objects
CoumPhOXA$_{31}$-MOXA$_{65}$		30 – 50 nm spheres + presence of aggregates
(Pheo)CoumPhOXA$_{31}$-MOXA$_{65}$	Pheo-loaded	
CoumPhOXA$_{31}$-MOXA$_{65}$ / X2080	with crosslinker (X2080) but uncrosslinked	i.e.
(Pheo) CoumPhOXA$_{31}$-MOXA$_{65}$ / X2080	Pheo-loaded, with crosslinker (X2080) but uncrosslinked	
X CoumPhOXA$_{31}$-MOXA$_{65}$ / X2080	crosslinked (X)	i.e.
(Pheo) X CoumPhOXA$_{31}$-MOXA$_{65}$ / X2080	Pheo-loaded, crosslinked (X)	
MePhOXA$_{31}$-MOXA$_{65}$		30 nm spheres
4-MU	Free coumarin	200 nm objects
CoumPhOXA$_{64}$-MOXA$_{104}$		40—–60 nm spheres
(Pheo)CoumPhOXA$_{64}$-MOXA$_{104}$	Pheo-loaded	
CoumPhOXA$_{64}$-MOXA$_{104}$ / X2080	with crosslinker (X2080) but uncrosslinked	Spheres and elongated objects
(Pheo) CoumPhOXA$_{64}$-MOXA$_{104}$ / X2080	Pheo-loaded, with crosslinker (X2080) but uncrosslinked	
X CoumPhOXA$_{64}$-MOXA$_{104}$ / X2080	crosslinked (X)	Spheres and elongated objects
(Pheo) X CoumPhOXA$_{64}$-MOXA$_{104}$ / X2080	Pheo-loaded, crosslinked (X)	
CoumPhOXA$_5$-MOXA$_{68}$		Low number of 9 – 300 nm objects
(Pheo)CoumPhOXA$_5$-MOXA$_{68}$	Pheo-loaded	
CoumPhOXA$_5$-MOXA$_{68}$ / X2080	with crosslinker (X2080) but uncrosslinked	30–200 nm low number of objects
(Pheo) CoumPhOXA$_5$-MOXA$_{68}$ / X2080	Pheo-loaded, with crosslinker (X2080) but uncrosslinked	
X CoumPhOXA$_5$-MOXA$_{68}$ / X2080	crosslinked (X)	40–200 nm low number of objects
(Pheo) X CoumPhOXA$_5$-MOXA$_{68}$ / X2080	Pheo-loaded, crosslinked (X)	
CoumBuOXA$_9$-MOXA$_{94}$		15–400 nm low number of objects
(Pheo)CoumBuOXA$_9$-MOXA$_{94}$	Pheo-loaded	
CoumBuOXA$_9$-MOXA$_{94}$/ X2080	with crosslinker (X2080) but uncrosslinked	25–400 nm low number of objects
(Pheo) CoumBuOXA$_9$-MOXA$_{94}$/ X2080	Pheo-loaded, with crosslinker (X2080) but uncrosslinked	
X CoumBuOXA$_9$-MOXA$_{94}$/ X2080	crosslinked (X)	20–400 nm low number of objects
(Pheo) X CoumBuOXA$_9$-MOXA$_{94}$/ X2080	Pheo-loaded, crosslinked (X)	
CoumPhOXA$_{80}$-MOXA$_{65}$		85 nm spheres
(Pheo)CoumPhOXA$_{80}$-MOXA$_{65}$	Pheo-loaded	
CoumPhOXA$_{80}$-MOXA$_{65}$ / X2080	with crosslinker (X2080) but uncrosslinked	90 nm spheres
(Pheo) CoumPhOXA$_{80}$-MOXA$_{65}$ / X2080	Pheo-loaded, with crosslinker (X2080) but uncrosslinked	
X CoumPhOXA$_{80}$-MOXA$_{65}$ / X2080	crosslinked (X)	90 nm spheres

(*continued on next page*)

Table 1 (*continued*)

Notation	Description	Characteristics*
(Pheo) X CoumPhOXA$_{80}$-MOXA$_{65}$ / X2080	Pheo-loaded, crosslinked (X)	

a coumarin-functionalized macromolecular crosslinker named X2080 in relation to its composition (20 % of ethylhexylmethacrylate vs 80 % of the coumarin methacrylate repeating unit) and the self-assemblies were obtained by film rehydration followed by ultrasonication at 37 kHz. When needed, they were then crosslinked under UV illumination, leading to 95 % dimerized coumarin units as observed by 1H NMR, after freeze-drying of water and redispersion in CDCl3 (Belkhir et al., 2022). Encapsulation of Pheo as photosensitizer was performed by adding a low and known amount of Pheo solution in acetone to the polyoxazoline nanovector solution, followed by a 2-day evaporation of acetone. Tables 1 and S1 present all systems used in this study, together with their characteristics. For the naming of each system, /X2080 indicates that the cross-linker was present, the presence of X in front of the name indicates that the system was crosslinked. (Pheo) in front of the name indicates that Pheo was loaded into the nanovector. For instance, CoumPhOXA$_{31}$-MOXA$_{65}$ represents the poly(2-oxazoline) copolymer alone, CoumPhOXA$_{31}$-MOXA$_{65}$/X2080 the vector formed in the presence of the cross-linker but the vector remains un-crosslinked. Finally, X CoumPhOXA$_{31}$-MOXA$_{65}$/X20-80 stands for this same vector which has been crosslinked. All systems were characterized by Dynamic Light Scattering (DLS) and Transmission Electron Microscopy (TEM). Figs. 1 and S10 present those for CoumPhOXA$_{31}$-MOXA$_{65}$ as an example. Encapsulation of Pheo in the nanovectors did not induce any morphology modification. All characterizations are provided in supplementary information (Figures S11-17). The asset of the selected nanovector set is to provide us with a variety of morphologies while keeping the chemistry constant. Indeed, depending on the hydrophilic fraction and the molar mass of the polymers, nanovectors were either spherical (CoumPhOXA$_{31}$-MOXA$_{65}$, CoumPhOXA$_{80}$-MOXA$_{65}$) or a mixture of spheres and elongated systems (CoumPhOXA$_{64}$-MOXA$_{104}$). The amount of formed nanovectors was also modified depending on the hydrophilic fraction. In the case of most hydrophilic polymers (CoumPhOXA$_5$-MOXA$_{68}$, CoumBuOXA$_9$-MOXA$_{94}$), they were only scarcely observable by TEM, indicative of a large amount of soluble polymer. Finally, CoumPhOXA$_{80}$-MOXA$_{65}$ provided larger nanovectors compared to the other systems. Figure S9 shows the DLS analysis of different batches for different polymers, giving an indication of the good reproducibility of the process. The nanovectors were observed to be stable over at least 5 weeks at room temperature, as illustrated in supplementary information (Figure S18) in the case of CoumPhOXA$_{31}$-MOXA$_{65}$. As further discussed in the text, a polymer without any coumarin group, MePhOXA$_{31}$-MOXA$_{65}$, was also synthesized to assess the influence of this group. The formation of the self-assemblies was comparable to that of CoumPhOXA$_{31}$-MOXA$_{65}$. Encapsulation of Pheo was confirmed by UV–vis spectroscopy, as already published (Oudin et al., 2019), by the shift of absorbance from 690 nm in water to 670 nm in a more hydrophobic environment such as polyoxazolines (Fig S19). The UV–visible spectra indicated that all Pheo present was encapsulated and none remained free in water.

3.2. Evaluation of cyto- and photo-toxicity

In order to assess the efficiency of the nanovectors in PDT protocols, the first step was to evaluate the cytotoxicity of the systems including those without any Pheo. Over the range of concentrations tested, from 7.8 nM to 1 μM Pheo equivalent, the different nanovectors, whether empty or loaded with Pheo, showed no cytotoxicity on HCT-116 cells (Fig. 2A). From now on, a typical concentration of 0.125 μM will be analyzed to compare cell viability as a function of treatments. At this concentration, only the (Pheo)CoumPhOXA$_{64}$-MOXA$_{104}$ condition induced a very slight proliferation of cells ($p = 0.0211$) compared with

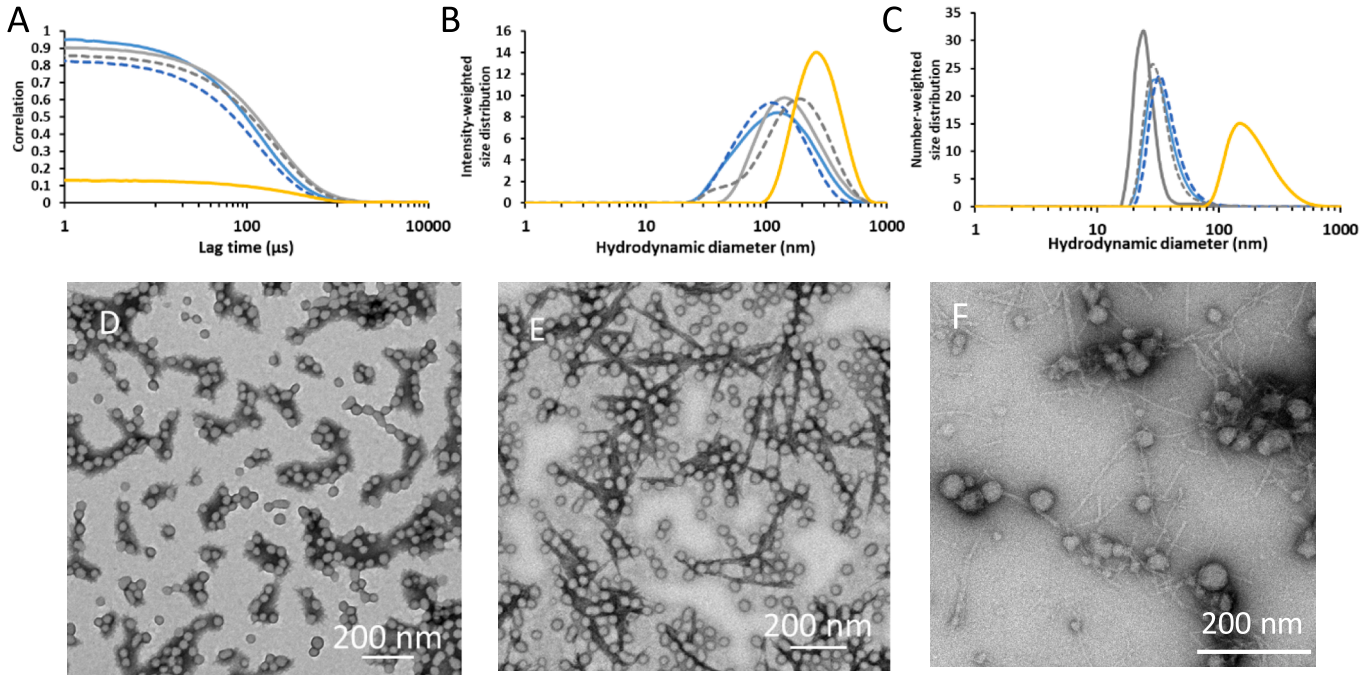

Fig. 1. Characterization of CoumPhOXA$_{31}$-MOXA$_{65}$ nanovectors loaded or not with Pheo. Comparison of the objects formed from Pheo alone in water. Blue line CoumPhOXA$_{31}$-MOXA$_{65}$, grey line X CoumPhOXA$_{31}$-MOXA$_{65}$/X2080, dotted blue line CoumPhOXA$_{31}$-MOXA$_{65}$ + Pheo, dotted grey line X CoumPhOXA$_{31}$-MOXA$_{65}$/X2080 + Pheo, yellow line Pheo alone. A. DLS characterization, correlograms; B. DLS characterization, intensity-weighted distribution; C. DLS characterization, number-weighted distribution. D. TEM of CoumPhOXA$_{31}$MOXA$_{65}$; E. TEM of CoumPhOXA$_{31}$-MOXA$_{65}$ + Pheo; F. TEM of Pheo alone. The TEM histograms are given in Fig. S8 except for the Pheo alone condition, which shows a mixture of elongated and more regular shapes.

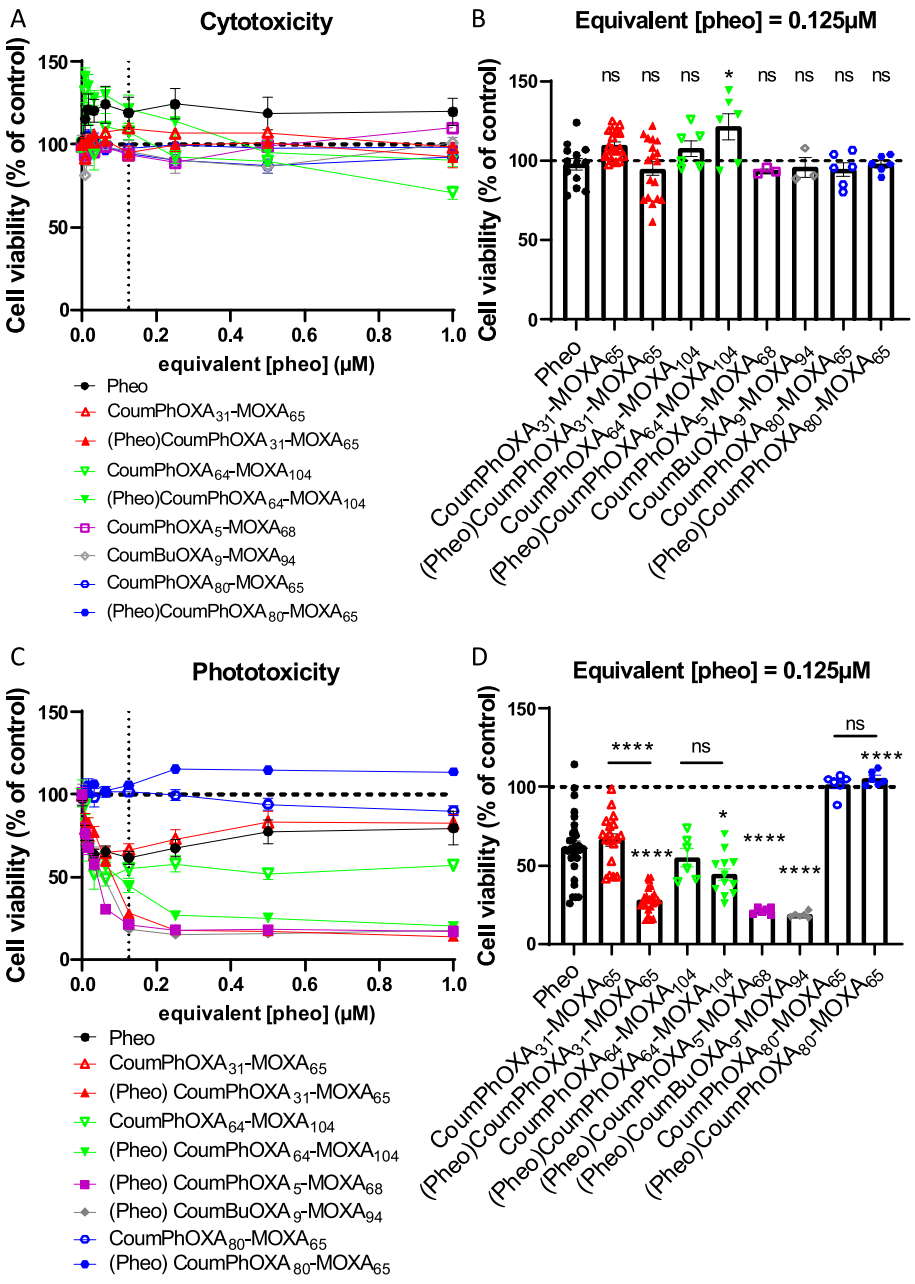

Fig. 2. Cytotoxicity and phototoxicity of empty or pheo-loaded polymeric nanovectors on HCT-116 human tumor cells. Cell viability was quantified by Prestoblue assay 24 h after incubation with nanovectors at equivalent Pheo concentrations from 7.8 nM to 1 µM to determine cytotoxicity (A) or phototoxicity (C). A specific focus on low concentration [pheo] = 0.125 µM is performed respectively in cytotoxicity (B) and phototoxicity (D) experiments. Empty symbols: empty nanovectors. Filled symbols: pheo-loaded nanovectors. For (B) and (D), individual biological replicates are represented ± SEM, and analyzed by 1-way ANOVA followed by Tukey's multiple comparisons test against free pheo condition or between paired (empty/pheo-loaded) nanovectors.

the free Pheo condition (Fig. 2B). It is therefore clear that in the absence of light activation, polymer self-assemblies, whether empty or Pheo-loaded, were not cytotoxic. The same series of experiments was carried out under light irradiation to determine the phototoxicity of these same nanovectors, whether empty or Pheo-loaded (Fig. 2C). Four behaviors emerged. Pheo alone induced at best an average decrease of 40 % in cell viability, at a concentration of 0.125 µM. From one experiment to another, the aggregates formed by free Pheo by π-π stacking were not identical (Figure S20), owing to the low repeatability of nano-precipitation of such system without any stabilizer, which explains the wide variability in the biological viability data collected over 5 independent experiments. CoumPhOXA$_{80}$-MOXA$_{65}$ polymer-based nanovectors, whether empty or loaded with Pheo, did not affect cell viability. Compared with the other objects in this study, these nanoparticles were very large (around 80 nm in diameter), which could explain their smaller surface area for interaction with cell membranes and therefore their limited penetration/internalization. CoumPhOXA$_5$-MOXA$_{68}$ and CoumBuOXA$_9$-MOXA$_{94}$ based Pheo-loaded objects were undoubtedly the most effective in reducing cell viability once photo-activated. However, as these polymers are very hydrophilic, their self-organization is poorly defined, and we cannot ascertain that the observed efficiency is linked to the soluble polymers or the self-assemblies. Indeed, from additional characterization by Field Flow Fractionation (data to be published), we were able to prove the presence of unimers.

Finally, the two polymers CoumPhOXA$_{31}$-MOXA$_{65}$ and

CoumPhOXA$_{64}$-MOXA$_{104}$ showed the same type of behaviour, i.e. significant phototoxicity for empty nanovectors, significantly enhanced in the case of CoumPhOXA$_{31}$-MOXA$_{65}$ loaded with Pheo, whereas this was only a trend (not statistically different) for (Pheo)CoumPhOXA$_{64}$-MOXA$_{104}$. There are two important points to note from this experience. Firstly, self-assemblies based on these two polymers exhibit phototoxicity even in the absence of a photosensitizer. This point will be discussed in the next paragraph. Secondly, these nanovectors are effective in improving the anti-tumour efficacy of the photosensitizer when encapsulated, unlike the CoumPhOXA$_{80}$-MOXA$_{65}$ family. The potential of poly(2-oxazolines) as nanovectors therefore expectedly depends on their physicochemical specificities.

3.3. Influence of the coumarin group in the phototoxicity of the different systems

To go further and understand the observed phototoxicity of the empty nanovectors, in particular the role of the coumarin moiety, we focused on PhOXA$_{31}$-MOXA$_{65}$ and synthesized a polymer with the same specificities but without the coumarin function: MePhOXA$_{31}$-MOXA$_{65}$. In parallel, 4-methylumbelliferone (4-MU) also known as 7-hydroxy-4-methylcoumarin was used as a control for the coumarin component (Scheme 1). Indeed, as already mentioned in introduction, coumarins are known to display a wide range of biological and pharmaceutical effects, including antibacterial, antifungal, antiviral, anti-HIV and anticancer activities (Hussain et al., 2019), as well as photosensitizer abilities in PDT application (Ortega-Forte et al., 2021). Coumarins, fluorescent heterocyclic compounds, were reported in a large variety of fluorescence application as well as photoinitiators thanks to their wide variety of electronic, photochemical and photophysical properties (Abdallah et al., 2019). Coumarins and their derivatives are sensitive to near-UV and blue light (Goodwin and Pollock, 1954).

In a dedicated set of experiments, we compared PhOXA$_{31}$-MOXA$_{65}$, MePhOXA$_{31}$-MOXA$_{65}$ and 4-MU without and with light irradiation (Fig. 3). We chose to work at same concentration as in previous figures, namely equivalent [pheo] = 0.125 μM. It should be noted that in the absence of light, none of the tested elements induced cytotoxicity. Under visible light irradiation, the empty CoumPhOXA$_{31}$-MOXA$_{65}$ nanovectors alone induced around 20 % of phototoxicity, as observed in Fig. 2 with a different set of experimental data. Nanovectors formed with polymers containing no coumarin function, MePhOXA$_{31}$-MOXA$_{65}$, did not show any phototoxicity, on the contrary, a pro-proliferative effect of these nanovectors was observed but not explained yet. These results indicate that it is indeed the coumarin function that is responsible for the observed phototoxicity. Finally, coumarin in its free form (4-MU) did not affect cell viability. 4-MU maximum excitation wavelength is 380 nm in water (Snavely et al., 1967); since the illumination system we used filters out wavelengths above 400 nm, 4-MU was presumably not efficiently photoactivated, which explains the absence of phototoxicity observed. Another possible explanation could be that 4-MU aggregates are not phototoxic versus a well dissolved molecule. These results clearly show the benefit of including an active coumarin unit in the polymer forming the nanovector.

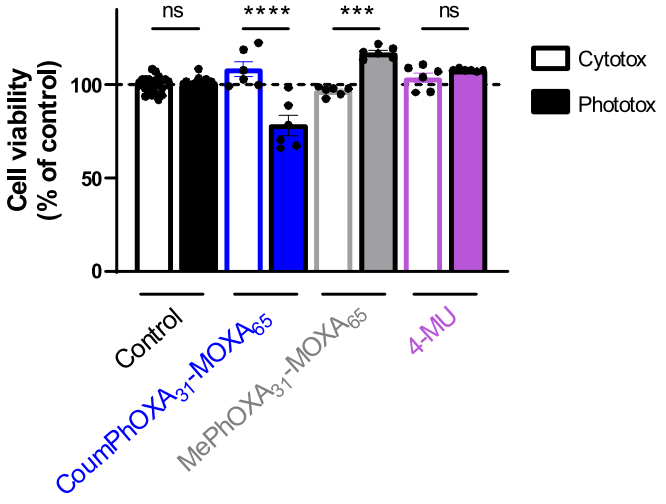

Fig. 3. Cytotoxicity and phototoxicity of coumarin function in empty polymeric nanovectors on HCT-116 human tumor cells. Cell viability was quantified by Prestoblue assay 24 h after incubation with nanovectors 3.75 μM CoumPhOXA$_{31}$-MOXA$_{65}$, MePhOXA$_{31}$-MOXA$_{65}$ or coumarin alone (4-MU). Coumarin in 4-MU is at equivalent concentration than coumarin concentration in CoumPhOXA$_{31}$-MOXA$_{65}$. Individual biological replicates are represented ± SEM, and analyzed by 1-way ANOVA followed by Tukey's multiple comparisons test between paired non-irradiated (empty bar, Cytotox) and irradiated (full bar, Phototox) conditions. 4-MU: 4-Methylumbelliferone.

3.4. Influence of the crosslinking

Crosslinking of nanovectors has been repeatedly suggested in the literature to optimize their stability and sustainability. The formulation used here can be crosslinked by UV irradiation, owing to the possible dimerization of coumarin. To study the benefit of crosslinking nanovectors for therapeutic efficacy, we established the following strategy: for each polymer family, the cellular response in terms of phototoxicity was evaluated by comparing the efficacy of free Pheo, the unmodified polymer nanovectors, called 'basic', the nanovectors in the presence of cross-linker X2080 but not cross-linked (to ensure the absence of crosslinker effect), and finally the crosslinked nanovectors. Only Pheo-loaded- CoumPhOXA$_{31}$-MOXA$_{65}$, CoumPhOXA$_{64}$-MOXA$_{104}$ and CoumPhOXA$_{80}$-MOXA$_{65}$ families are presented in the main text (Fig. 4). The results for CoumPhOXA$_{5}$-MOXA$_{68}$ and CoumBuOXA$_{9}$-MOXA$_{94}$ hydrophilic families, for which the characterization of the objects is not certain, are shown in SI (Figure S21). For ease of reading, we have chosen to compare the biological results by polymer family, but a comparison by group (basic, uncrosslinked in the presence of crosslinker X2080, crosslinked) is available in SI (Figures S22-24). With regard to the (Pheo)CoumPhOXA$_{31}$-MOXA$_{65}$ family, it appears that, whatever Pheo concentration, the basic version of the polymer is more effective in affecting cell viability than free Pheo and the modified versions of the nanovector (uncrosslinked in the presence of crosslinker X2080 and crosslinked), except for the highest concentration tested at 1 μM (Fig. 4A). This is particularly true at the reference concentration we chose (i.e. 0.125 μM). With regard to the (Pheo)CoumPhOXA$_{64}$-MOXA$_{104}$ family, photoxicity curves were similar and almost superimposed, indicating no difference between the efficacy of basic nanovectors and their crosslinked form, which was confirmed by the statistical analysis at Pheo concentration 0.125 μM (Fig. 4B). Finally, as observed previously for cytotoxicity/phototoxicity experiment with basic polymer (Fig. 3), the (Pheo)CoumPhOXA$_{80}$-MOXA$_{65}$, in presence of crosslinker X2080 or crosslinked, did not alter the cell viability. This means that neither in this case did crosslinking add value to the potential of the nanocarrier for photodynamic therapy.

From these results we can conclude that for this class of nanovectors, the addition of a cross-linking agent is not beneficial for PDT. In the case of (Pheo)CoumPhOXA$_{31}$-MOXA$_{65}$ family it is even detrimental. Many parameters can affect the PDT efficiency in the presence of a nanovector and at this point of the investigation it is difficult to discriminate the role of each of them: shape, size and stability of the nanovector, photosensitizer concentration inside the cells and in this particular case also the concentration of coumarin units and the effect of cross-linking on their phototoxic effect. Indeed, crosslinking or the presence of the cross-linking agent alters the conformation of the coumarin function, which could therefore be no longer available to display this phototoxic effect. One main conclusion is that stability improvement is not a main issue in this class of materials, the presence of aromatic units which can induce π-π stacking guarantee a sufficient stability of the nanovectors.

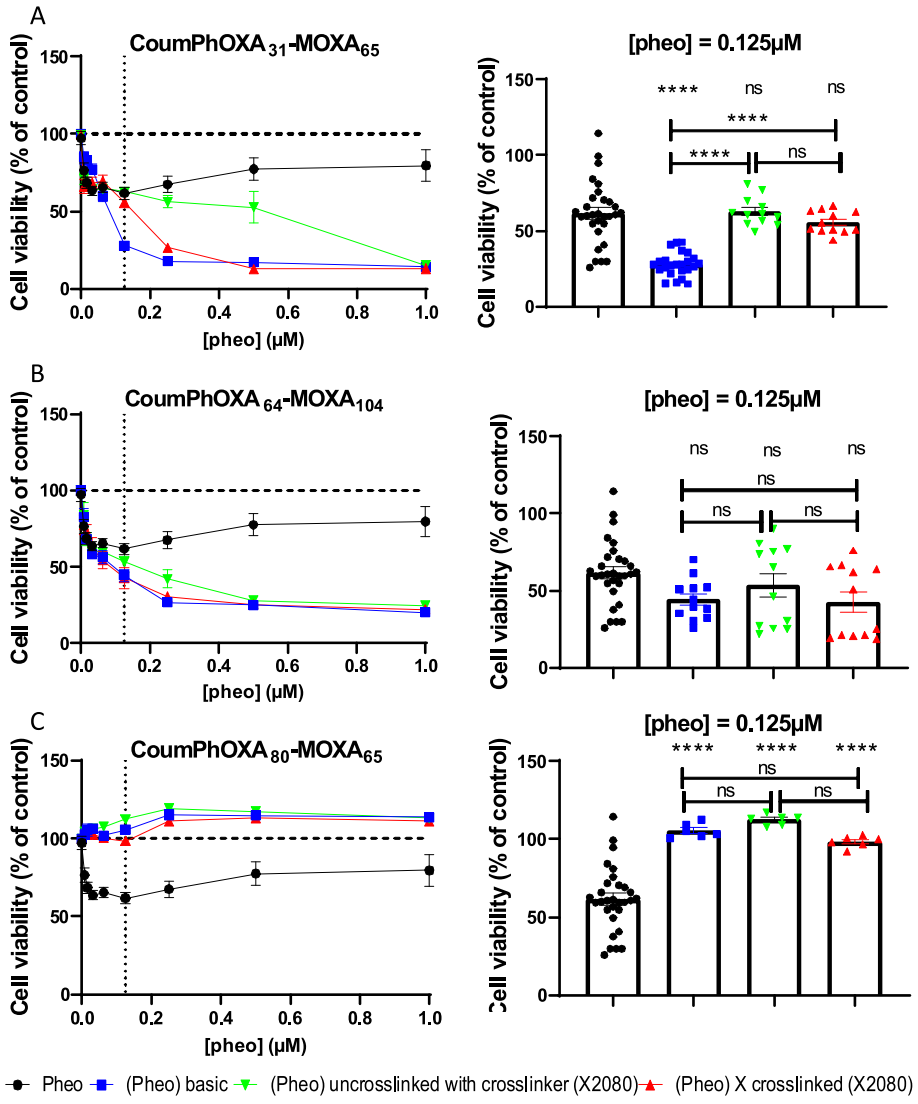

Fig. 4. Phototoxicity of pheo-loaded uncrosslinked and crosslinked polymeric nanovectors on HCT-116 human tumor cells. Cell viability was quantified by Prestoblue assay 24 h after incubation with nanovectors at equivalent Pheo concentrations from 7.8 nM to 1 μM (left column) and at [pheo] = 0.125 μM (right column). A. Pheo-loaded CoumPhOXA$_{31}$-MOXA$_{65}$ family. B. Pheo-loaded CoumPhOXA$_{64}$-MOXA$_{104}$ family. C. Pheo-loaded CoumPhOXA$_{80}$-MOXA$_{65}$ family. Black point: free pheophorbide condition; Blue squares: pheo-loaded basic (non-modified) nanovectors; green inversed triangles: pheo-loaded uncrosslinked nanovectors in presence of X2080 crosslinker; red triangles: pheo-loaded crosslinked nanovectors. For right column, individual biological replicates are represented ± SEM, and analyzed by 1-way ANOVA followed by Tukey's multiple comparisons test against free pheo condition or between paired nanovectors.

It is important to keep in mind that these results were obtained on cells cultured in monolayer and the conclusions must therefore be nuanced. Indeed, in 2D culture, cell membranes are easily exposed and in contact with therapeutic agent incubated in cell culture medium, contrary to 3D cell culture like spheroids for example. In these 3D cultures, cells are grown in the 3 dimensions and display complex cell–cell junctions and cell–ECM interactions which better mimic the specificity of native tissues (Pampaloni et al., 2007). 3D cell cultures are currently used in a broad range of researches, including cell biology, tumor biology, epithelial morphogenesis, drug screening, and nanoparticle evaluation (Lu and Stenzel, 2018). In a previous work on the effect of crosslinking of polymeric nanovectors based on PEO-PCL (Till et al., 2016b), we had underlined that the crosslinking did not significantly improve the effectiveness of the treatment by PDT on monolayers, whereas in a 3D context (tumor spheroids) it brought added value. It would therefore be interesting to evaluate all or part of the nanovectors that we have developed, crosslinked or not, on 3D tumor spheroids, but this perspective goes beyond our current study.

3.5. Evaluation of protein corona

Due to the established role of protein corona (PC) on nanovectors fate *in vivo*, characterizing nanovectors biological identity is essential for the development of safe and effective delivery systems. As already mentioned, PEO-based nanovectors, although recognized as stealth systems, can lead in some cases to immunologic reactions, due to possible recognition by specific proteins. Moreover, given the hydrophilic nature of the poly(2-methyl-2-oxazoline) exposed on the presented nanovectors surface, potentially leading to protein adsorption, it was important for us to characterize nanovectors behavior in protein containing media, in terms of colloidal stability and protein corona formation.

We decided to focus on CoumPhOXA$_{31}$-MOXA$_{65}$ for this section. Specifically, CoumPhOXA$_{31}$-MOXA$_{65}$, CoumPhOXA$_{31}$-MOXA$_{65}$ / X2080 and XCoumPhOXA$_{31}$-MOXA$_{65}$ / X2080 were incubated for 30 min in DMEM + 10 % FBS. Then nanovectors/protein complexes were isolated by centrifugation in a 3–30 % sucrose gradient. Nanovectors localization in sucrose layers was evaluated by DLS analysis; the lack of free protein

contamination was instead confirmed by SDS-PAGE of the DMEM + 10 % FBS control (Figure S25), confirming that the excess of proteins from the media are exclusively located in lower density sucrose layers, thus differing from those enriched in nanovectors.

For all analyzed samples, DLS analysis showed no significative differences between NPs in water and upon 30 min incubation in DMEM + 10 % FBS, as suggested by the superimposition of the autocorrelation functions and comparable hydrodynamic radius distributions (Fig. 5A-H). This indicated the colloidal stability of the nanovectors in protein-containing media and suggested a stealth character. Stealth properties were further confirmed by electrophoresis. Specifically, SDS-PAGE performed on the nanovectors-containing protein fractions, isolated from excess proteins by ultracentrifugation with sucrose gradient (layers 7 and 6) showed the lack of visible protein bands, confirming the absence of a consistent protein corona formation (Fig. 5C, F, I).

4. Conclusion

In summary, we have shown that nanovectors based on amphiphilic poly(2-oxazoline)s are efficient for encapsulating Pheophorbide a, a photosensitizer for PDT. PDT on HCT-116 cancer cells is strongly improved upon encapsulation, compared to the use of Pheo alone without any formulation. Furthermore, the presence of coumarin units on the polymers enables a synergy in the photocytotoxicity coming from the intrinsic properties of coumarin groups. This provides a further improvement of the treatment. Coumarin units also enable to crosslink the nanovectors. In our case, based on 2D cell cultures, this did not provide any further gain. To go further and get closer to the constraints of native *in vivo* tissues (3D organization of dense intercellular junctions, etc.), further work could focus on the therapeutic efficacy of our nanovectors in 3D tumor spheroids. In this context, the literature points to the added value of cross-linking drug delivery systems, which are more likely to remain intact and therefore more effective than their non-crosslinked counterparts. Finally, these nanovectors were shown not to lead to the formation of a protein corona. As with nanovectors decorated with poly(ethylene glycol), the absence of protein corona should prevent these systems from being recognized by the innate immune system and therefore prevent rapid elimination during the first hepatic passage, making them promising stealth nanovectors for *in vivo* applications. However, there is increasing evidence for unexpected immune responses occurring against pegylated nanocarriers upon repeated administration, an issue becoming more relevant considering the recently running SARS-CoV2 vaccination campaigns. Thus, it would be necessary to verify these types of detrimental biological responses to

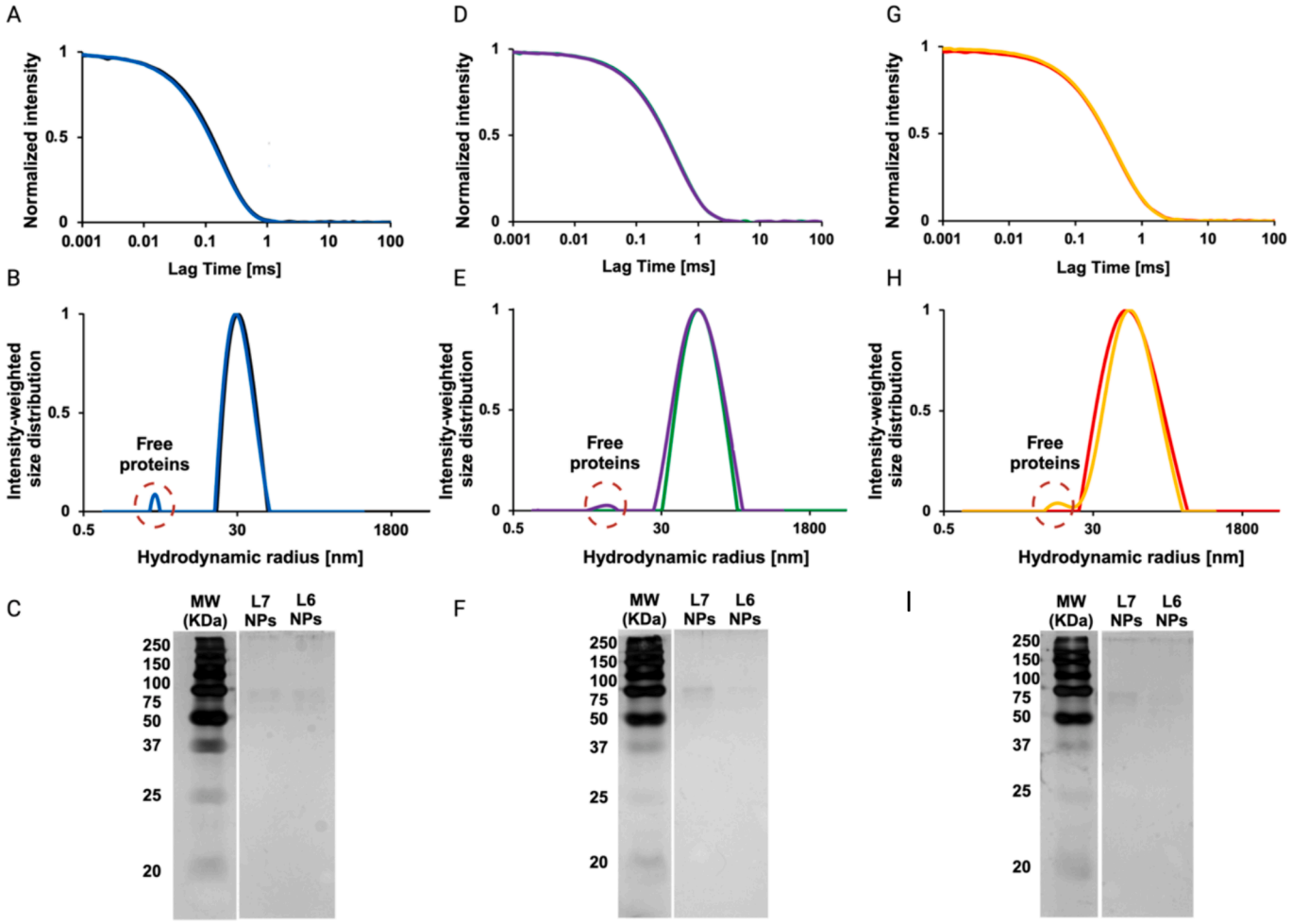

Fig. 5. NPs protein corona evaluation by DLS and SDS-PAGE. A. Autocorrelation function and B. hydrodynamic radius (R_H, nm) of CoumPhOXA$_{31}$-MOXA$_{65}$ in water (black line) and upon 30 min incubation in DMEM + 10 % FBS (blue line); C. SDS-PAGE of CoumPhOXA$_{31}$-MOXA$_{65}$-PC complexes isolated with sucrose gradient centrifugation method (layers 7 and 6). D. Autocorrelation function and E. hydrodynamic radius (R_H, nm) of CoumPhOXA$_{31}$-MOXA$_{65}$ / X2080 in water (green line) and upon 30 min incubation in DMEM + 10 % FBS (purple line); F. SDS-PAGE of CoumPhOXA$_{31}$-MOXA$_{65}$ / X2080-PC complexes isolated with sucrose gradient centrifugation method (layers 7 and 6). G. Autocorrelation function and H. Hydrodynamic radius (R_H, nm) of XCoumPhOXA$_{31}$-MOXA$_{65}$ / X2080 in water (red line) and upon 30 min incubation in DMEM + 10 % FBS (yellow line); I. SDS-PAGE of CoumPhOXA$_{31}$-MOXA$_{65}$ / X2080-PC complexes isolated with sucrose gradient centrifugation method (layers 7 and 6).

POx-decorated nanovectors. Indeed, progress in nanomedicine will be obtained only by comparing and confronting different nanovectors for the same application. Beyond PDT, such nanovectors could also be used for any application for which photocontrolled of the crosslinking can be useful. Here, we have only used the dimerization of coumarin. Uncrosslinking could be performed by illumination below 290 nm, for instance in diagnostics.

CRediT authorship contribution statement

Diana Heaugwane: Writing – review & editing, Investigation, Formal analysis. **Orélia Cerlati:** Investigation. **Kedafi Belkhir:** Investigation. **Belkacem Tarek Benkhaled:** Investigation. **Sylvain Catrouillet:** Writing – review & editing, Conceptualization. **Isabelle Fabing:** Writing – review & editing, Investigation. **Catherine Claparols:** Investigation. **Marc Vedrenne:** Investigation. **Dominique Goudounèche:** Investigation. **Bruno Payré:** Investigation. **Beatrice Lucia Bona:** Writing – review & editing, Investigation. **Alice Tosi:** Investigation. **Francesca Baldelli Bombelli:** Supervision. **Patricia Vicendo:** Writing – review & editing, Conceptualization. **Vincent Lapinte:** Writing – review & editing, Supervision, Funding acquisition, Conceptualization. **Barbara Lonetti:** Writing – review & editing, Conceptualization. **Anne-Françoise Mingotaud:** Writing – review & editing, Writing – original draft, Supervision, Funding acquisition, Conceptualization. **Laure Gibot:** Writing – review & editing, Writing – original draft, Supervision, Formal analysis, Conceptualization.

Declaration of competing interest

The authors declare that they have no known competing financial interests or personal relationships that could have appeared to influence the work reported in this paper.

Data availability

Data will be made available on request.

Acknowledgment

We would like to acknowledge the Occitanie Region and EU for their financial support (FEDER LR0021768: Pheophotodyn). The analysis by UHPLC were recorded on Acquity UPLC, from Waters, which are part of the “Integrated Screening Platform of Toulouse” (PICT, GenoToul, IBiSA).

Appendix A. Supplementary material

Synthesis of MePhOXA$_{31}$-MOXA$_{65}$, characteristics of the polymers, characterization of Pheo, DLS and TEM data for the nanovectors, stability with time of nanovector solutions, absorption spectrum of Pheo alone in water and in different nanovectors, DLS analysis of different batches for Pheo alone, phototoxicity of pheo-loaded uncrosslinked and crosslinked hydrophilic polymer on HCT-116 human tumor cells, phototoxicity of pheo-loaded basic polymer on HCT-116 human tumor cells, phototoxicity of pheo-loaded uncrosslinked polymer nanovectors in presence of crosslinker X2080 on HCT-116 human tumor cells, phototoxicity of pheo-loaded crosslinked polymer nanovectors on HCT-116 human tumor cells, SDS-PAGE of DMEM + 10 % FBS without the addition of nanovectors. Supplementary data to this article can be found online at https://doi.org/10.1016/j.ijpharm.2024.124186.

References

Abdallah, M., Hijazi, A., Graff, B., Fouassier, J.-P., Rodeghiero, G., Gualandi, A., Dumur, F., Cozzi, P.G., Lalevée, J., 2019. Coumarin derivatives as versatile photoinitiators for 3D printing, polymerization in water and photocomposite synthesis. Polym. Chem. 10, 872–884. https://doi.org/10.1039/C8PY01708E.

Al-Warhi, T., Sabt, A., Elkaeed, E.B., Eldehna, W.M., 2020. Recent advancements of coumarin-based anticancer agents: an up-to-date review. Bioorg. Chem. 103, 104163 https://doi.org/10.1016/j.bioorg.2020.104163.

Annunziata, F., Pinna, C., Dallavalle, S., Tamborini, L., Pinto, A., 2020. An overview of coumarin as a versatile and readily accessible Scaffold with broad-ranging biological activities. Int. J. Mol. Sci. 21, 4618. https://doi.org/10.3390/ijms21134618.

Belkhir, K., Cerlati, O., Heaugwane, D., Tosi, A., Benkhaled, B.T., Brient, P.-L., Chatard, C., Graillot, A., Catrouillet, S., Balor, S., Goudounèche, D., Payré, B., Laborie, P., Lim, J.-H., Putaux, J.-L., Vicendo, P., Gibot, L., Lonetti, B., Mingotaud, A.-F., Lapinte, V., 2022. Synthesis and Self-assembly of UV-crosslinkable amphiphilic polyoxazoline block copolymers: importance of multitechnique characterization. Langmuir 38, 16144–16155. https://doi.org/10.1021/acs.langmuir.2c02896.

Bonelli, J., Ortega-Forte, E., Rovira, A., Bosch, M., Torres, O., Cuscó, C., Rocas, J., Ruiz, J., Marchán, V., 2022. Improving photodynamic therapy anticancer activity of a mitochondria-targeted coumarin photosensitizer using a polyurethane-polyurea hybrid nanocarrier. Biomacromolecules 23, 2900–2913. https://doi.org/10.1021/acs.biomac.2c00361.

Cagliani, R., Gatto, F., Bardi, G., 2019. Protein adsorption: a feasible method for nanoparticle functionalization? Materials 12, 1991. https://doi.org/10.3390/ma12121991.

Cazin, I., Rossegger, E., Guedes de la Cruz, G., Griesser, T., Schlögl, S., 2021. Recent advances in functional polymers containing coumarin chromophores. Polymers 13, 56. https://doi.org/10.3390/polym13010056.

Chang, H., Liu, Y., Shi, M., Liu, Z., Liu, Z., Jiang, J., 2015. Photo-induced dynamic association of coumarin pendants within amphiphilic random copolymer micelles. Colloid Polym Sci 293, 823–831. https://doi.org/10.1007/s00396-014-3474-7.

Coty, J.-B., Vauthier, C., 2018. Characterization of nanomedicines: a reflection on a field under construction needed for clinical translation success. J. Control. Release 275, 254–268. https://doi.org/10.1016/j.jconrel.2018.02.013.

Danner, A.-K., Schöttler, S., Alexandrino, E., Hammer, S., Landfester, K., Mailänder, V., Morsbach, S., Frey, H., Wurm, F.R., 2019. Phosphonylation controls the protein corona of multifunctional polyglycerol-modified nanocarriers. Macromol. Biosci. 19, 1800468. https://doi.org/10.1002/mabi.201800468.

Das, R.P., Gandhi, V.V., Singh, B.G., Kunwar, A., 2019. Passive and active drug targeting: role of nanocarriers in rational design of anticancer formulations. Curr. Pharm. Des. 25, 3034–3056. https://doi.org/10.2174/1381612825666190830155319.

Digiacomo, L., Pozzi, D., Palchetti, S., Zingoni, A., Caracciolo, G., 2020. Impact of the protein corona on nanomaterial immune response and targeting ability. WIREs Nanomed. Nanobiotechnol. 12, e1615.

Escamilla-Rivera, V., Solorio-Rodríguez, A., Uribe-Ramírez, M., Lozano, O., Lucas, S., Chagolla-López, A., Winkler, R., De Vizcaya-Ruiz, A., 2019. Plasma protein adsorption on Fe3O4-PEG nanoparticles activates the complement system and induces an inflammatory response. Int. J. Nanomed. 14, 2055–2067. https://doi.org/10.2147/IJN.S192214.

Fan, W., Zhang, L., Li, Y., Wu, H., 2019. Recent progress of crosslinking strategies for polymeric micelles with enhanced drug delivery in cancer therapy. Curr. Med. Chem. 26, 2356–2376. https://doi.org/10.2174/0929867324666171121102255.

Garg, S.S., Gupta, J., Sharma, S., Sahu, D., 2020. An insight into the therapeutic applications of coumarin compounds and their mechanisms of action. Eur. J. Pharm. Sci. 152, 105424 https://doi.org/10.1016/j.ejps.2020.105424.

Gatti, L., Chirizzi, C., Rotta, G., Milesi, P., Sancho-Albero, M., Sebastián, V., Mondino, A., Santamaría, J., Metrangolo, P., Chaabane, L., Bombelli, F.B., 2023. Pivotal role of the protein corona in the cell uptake of fluorinated nanoparticles with increased sensitivity for 19F-MR imaging. Nanoscale Adv. 5, 3749–3760. https://doi.org/10.1039/D3NA00229B.

Gibot, L., Lemelle, A., Till, U., Moukarzel, B., Mingotaud, A.-F., Pimienta, V., Saint-Aguet, P., Rols, M.-P., Gaucher, M., Violleau, F., Chassenieux, C., Vicendo, P., 2014. Polymeric micelles encapsulating photosensitizer: structure/photodynamic therapy efficiency relation. Biomacromolecules 15, 1443–1455. https://doi.org/10.1021/bm5000407.

Goodwin, R.H., Pollock, B.M., 1954. Ultraviolet absorption spectra of coumarin derivatives. Arch. Biochem. Biophys. 49, 1–6. https://doi.org/10.1016/0003-9861(54)90162-9.

Grünebaum, J., Söbbing, J., Mulac, D., Langer, K., 2015. Nanoparticulate carriers for photodynamic therapy of cholangiocarcinoma: In vitro comparison of various polymer-based nanoparticles. Int. J. Pharm. 496, 942–952. https://doi.org/10.1016/j.ijpharm.2015.10.023.

Hussain, M.I., Syed, Q.A., Khattak, M.N.K., Hafez, B., Reigosa, M.J., El-Keblawy, A., 2019. Natural product coumarins: biological and pharmacological perspectives. Biologia 74, 863–888. https://doi.org/10.2478/s11756-019-00242-x.

Kaur, J., Gulati, M., Jha, N.K., Disouza, J., Patravale, V., Dua, K., Singh, S.K., 2022. Recent advances in developing polymeric micelles for treating cancer: breakthroughs and bottlenecks in their clinical translation. Drug Discov. Today 27, 1495–1512. https://doi.org/10.1016/j.drudis.2022.02.005.

Knop, K., Mingotaud, A.-F., El-Akra, N., Violleau, F., Souchard, J.-P., 2009. Monomeric pheophorbide (a)-containing poly (ethyleneglycol-b-ε-caprolactone) micelles for photodynamic therapy. Photochem. Photobiol. Sci. 8, 396–404. https://doi.org/10.1039/b811248g.

Korchia, L., Bouilhac, C., Lapinte, V., Travelet, C., Borsali, R., Robin, J.-J., 2015. Photodimerization as an alternative to photocrosslinking of nanoparticles: proof of concept with amphiphilic linear polyoxazoline bearing coumarin unit. Polym. Chem. 6, 6029–6039. https://doi.org/10.1039/C5PY00834D.

Korchia, L., Lapinte, V., Travelet, C., Borsali, R., Robin, J.-J., Bouilhac, C., 2017. UV-responsive amphiphilic graft copolymers based on coumarin and polyoxazoline. Soft Matter 13, 4507–4519. https://doi.org/10.1039/C7SM00682A.

Küpeli Akkol, E., Genç, Y., Karpuz, B., Sobarzo-Sánchez, E., Capasso, R., 2020. Coumarins and coumarin-related compounds in pharmacotherapy of cancer. Cancers 12, 1959. https://doi.org/10.3390/cancers12071959.

Lorson, T., Lübtow, M.M., Wegener, E., Haider, M.S., Borova, S., Nahm, D., Jordan, R., Sokolski-Papkov, M., Kabanov, A.V., Luxenhofer, R., 2018. Poly(2-oxazoline)s based biomaterials: a comprehensive and critical update. Biomaterials 178, 204–280. https://doi.org/10.1016/j.biomaterials.2018.05.022.

Lu, H., Stenzel, M.H., 2018. Multicellular tumor spheroids (MCTS) as a 3D in vitro evaluation tool of nanoparticles. Small 14, 1702858. https://doi.org/10.1002/smll.201702858.

Monopoli, M.P., Walczyk, D., Campbell, A., Elia, G., Lynch, I., Baldelli Bombelli, F., Dawson, K.A., 2011. Physical−chemical aspects of protein corona: relevance to in vitro and in vivo biological impacts of nanoparticles. J. Am. Chem. Soc. 133, 2525–2534. https://doi.org/10.1021/ja107583h.

Montis, C., Till, U., Vicendo, P., Roux, C., Mingotaud, A.-F., Violleau, F., Demazeau, M., Berti, D., Lonetti, B., 2018. Extended photo-induced endosome-like structures in giant vesicles promoted by block-copolymer nanocarriers. Nanoscale 10, 15442–15446. https://doi.org/10.1039/C8NR04355H.

Obaid, G., Broekgaarden, M., Bulin, A.-L., Huang, H.-C., Kuriakose, J., Liu, J., Hasan, T., 2016. Photonanomedicine: a convergence of photodynamic therapy and nanotechnology. Nanoscale 8, 12471–12503. https://doi.org/10.1039/C5NR08691D.

Ortega-Forte, E., Rovira, A., Gandioso, A., Bonelli, J., Bosch, M., Ruiz, J., Marchán, V., 2021. COUPY coumarins as novel mitochondria-targeted photodynamic therapy anticancer agents. J. Med. Chem. 64, 17209–17220. https://doi.org/10.1021/acs.jmedchem.1c01254.

Oudin, A., Chauvin, J., Gibot, L., Rols, M.-P., Balor, S., Goudounèche, D., Payre, B., Lonetti, B., Vicendo, P., Mingotaud, A.-F., 2019. Amphiphilic polymers based on polyoxazoline as relevant nanovectors for photodynamic therapy. J. Mater. Chem. B 7, 4973–4982. https://doi.org/10.1039/c9tb00118b.

Pampaloni, F., Reynaud, E.G., Stelzer, E.H., 2007. The third dimension bridges the gap between cell culture and live tissue. Nat Rev Mol Cell Biol 8, 839. https://doi.org/10.1038/nrm2236.

Qin, X., Li, Y., 2020. Strategies to design and synthesize polymer-based stimuli-responsive drug-delivery nanosystems. Chembiochem 21, 1236–1253. https://doi.org/10.1002/cbic.201900550.

Rampado, R., Crotti, S., Caliceti, P., Pucciarelli, S., Agostini, M., 2020. Recent advances in understanding the protein corona of nanoparticles and in the formulation of "stealthy" nanomaterials. Front. Bioeng. Biotechnol. 8 https://doi.org/10.3389/fbioe.2020.00166.

Ren, J., Andrikopoulos, N., Velonia, K., Tang, H., Cai, R., Ding, F., Ke, P.C., Chen, C., 2022. Chemical and Biophysical signatures of the protein corona in nanomedicine. J. Am. Chem. Soc. 144, 9184–9205. https://doi.org/10.1021/jacs.2c02277.

Rijcken, C.J.F., De Lorenzi, F., Biancacci, I., Hanssen, R.G.J.M., Thewissen, M., Hu, Q., Atrafi, F., Liskamp, R.M.J., Mathijssen, R.H.J., Miedema, I.H.C., Menke - van der Houven van Oordt, C.W., van Dongen, G.A.M.S., Vugts, D.J., Timmers, M., Hennink, W.E., Lammers, T., 2022. Design, development and clinical translation of CriPec®-based core-crosslinked polymeric micelles. Advanced Drug Delivery Reviews 191, 114613. doi: 10.1016/j.addr.2022.114613.

Ritz, S., Schöttler, S., Kotman, N., Baier, G., Musyanovych, A., Kuharev, J., Landfester, K., Schild, H., Jahn, O., Tenzer, S., Mailänder, V., 2015. Protein corona of nanoparticles: distinct proteins regulate the cellular uptake. Biomacromolecules 16, 1311–1321. https://doi.org/10.1021/acs.biomac.5b00108.

Schoppa, T., Jung, D., Rust, T., Mulac, D., Kuckling, D., Langer, K., 2021. Light-responsive polymeric nanoparticles based on a novel nitropiperonal based polyester as drug delivery systems for photosensitizers in PDT. Int. J. Pharm. 597, 120326 https://doi.org/10.1016/j.ijpharm.2021.120326.

Schöttler, S., Becker, G., Winzen, S., Steinbach, T., Mohr, K., Landfester, K., Mailänder, V., Wurm, F.R., 2016. Protein adsorption is required for stealth effect of poly(ethylene glycol)- and poly(phosphoester)-coated nanocarriers. Nature Nanotech 11, 372–377. https://doi.org/10.1038/nnano.2015.330.

Silvio, D.D., Rigby, N., Bajka, B., Mayes, A., Mackie, A., Bombelli, F.B., 2015. Technical tip: high-resolution isolation of nanoparticle–protein corona complexes from physiological fluids. Nanoscale 7, 11980–11990. https://doi.org/10.1039/C5NR02618K.

Snavely, B.B., Peterson, O.G., Reithel, R.F., 1967. Blue laser emission from a flashlamp-excited organic dye solution. Appl. Phys. Lett. 11, 275–276. https://doi.org/10.1063/1.1755132.

Tian, J., Zhang, W., 2019. Synthesis, self-assembly and applications of functional polymers based on porphyrins. Prog. Polym. Sci. 95, 65–117. https://doi.org/10.1016/j.progpolymsci.2019.05.002.

Till, U., Gibot, L., Mingotaud, C., Vicendo, P., Rols, M.-P., Gaucher, M., Violleau, F., Mingotaud, A.-F., 2016a. Self-assembled polymeric vectors mixtures: characterization of the polymorphism and existence of synergistic effects in photodynamic therapy. Nanotechnology 27, 315102. https://doi.org/10.1088/0957-4484/27/31/315102.

Till, U., Gibot, L., Vicendo, P., Rols, M.-P., Gaucher, M., Violleau, F., Mingotaud, A.-F., 2016b. Crosslinked polymeric self-assemblies as an efficient strategy for photodynamic therapy on a 3D cell culture. RSC Adv. 6, 69984–69998. https://doi.org/10.1039/C6RA09013C.

Velychkivska, N., Sedláček, O., Shatan, A.B., Spasovová, M., Filippov, S.K., Chahal, M.K., Janisova, L., Brus, J., Hanyková, L., Hill, J.P., Winnik, F.M., Labuta, J., 2022. Phase separation and pH-dependent behavior of four-arm star-shaped porphyrin-PNIPAM4 conjugates. Macromolecules 55, 2109–2122. https://doi.org/10.1021/acs.macromol.1c02188.

Verger, A., Brandhonneur, N., Molard, Y., Cordier, S., Kowouvi, K., Amela-Cortes, M., Dollo, G., 2021. From molecules to nanovectors: Current state of the art and applications of photosensitizers in photodynamic therapy. Int. J. Pharm. 604, 120763 https://doi.org/10.1016/j.ijpharm.2021.120763.

Wang, S., Zhang, J., Zhou, H., Lu, Y.C., Jin, X., Luo, L., You, J., 2023. The role of protein corona on nanodrugs for organ-targeting and its prospects of application. J. Control. Release 360, 15–43. https://doi.org/10.1016/j.jconrel.2023.06.014.

Zeng, L., Gao, J., Liu, Y., Gao, J., Yao, L., Yang, X., Liu, X., He, B., Hu, L., Shi, J., Song, M., Qu, G., Jiang, G., 2019. Role of protein corona in the biological effect of nanomaterials: Investigating methods. TrAC Trends Anal. Chem. 118, 303–314. https://doi.org/10.1016/j.trac.2019.05.039.

Zhao, N., Li, Y., Yin, W., Zhuang, J., Jia, Q., Wang, Z., Li, N., 2020. Controllable coumarin-based NIR fluorophores: selective subcellular imaging, cell membrane potential indication, and enhanced photodynamic therapy. ACS Appl. Mater. Interfaces 12, 2076–2086. https://doi.org/10.1021/acsami.9b18666.

Zheng, X., Lordon, B., Mingotaud, A.-F., Vicendo, P., Brival, R., Fourquaux, I., Gibot, L., Gallot, G., 2023. Terahertz spectroscopy sheds light on real-time exchange kinetics occurring through plasma membrane during photodynamic therapy treatment. Adv. Sci. 10, 2300589. https://doi.org/10.1002/advs.202300589.

Zou, Q., Fang, Y., Zhao, Y., Zhao, H., Wang, Y., Gu, Y., Wu, F., 2013. Synthesis and in vitro photocytotoxicity of coumarin derivatives for one- and two-photon excited photodynamic therapy. J. Med. Chem. 56, 5288–5294. https://doi.org/10.1021/jm400025g.